

mRNA Decay Proteins Are Targeted to poly(A)⁺ RNA and dsRNA-Containing Cytoplasmic Foci That Resemble P-Bodies in *Entamoeba histolytica*

Itzel López-Rosas¹, Esther Orozco^{1,2}, Laurence A. Marchat³, Guillermina García-Rivera², Nancy Guillen^{4,5}, Christian Weber^{4,5}, Eduardo Carrillo-Tapia¹, Olga Hernández de la Cruz¹, Carlos Pérez-Plasencia^{6,7}, César López-Camarillo^{1*}

1 Programa en Ciencias Genómicas, Universidad Autónoma de la Ciudad de México, México City, México, **2** Departamento de Infectómica y Patogénesis Molecular, Centro de Investigación y de Estudios Avanzados, Instituto Politécnico Nacional, México City, México, **3** Programa Institucional de Biomedicina Molecular y Red en Biotecnología, Escuela Nacional de Medicina y Homeopatía, Instituto Politécnico Nacional, México City, México, **4** Unité Biologie Cellulaire du Parasitisme, Institut Pasteur, Paris, France, **5** INSERM U786, Paris, France, **6** Unidad de Genómica y Secuenciación Masiva, Instituto Nacional de Cancerología, México City, México, **7** Unidad de Biomedicina, Facultad de Estudios Superiores-Iztacala, Universidad Nacional Autónoma de México, México City, México

Abstract

In higher eukaryotes, mRNA degradation and RNA-based gene silencing occur in cytoplasmic foci referred to as processing bodies (P-bodies). In protozoan parasites, the presence of P-bodies and their putative role in mRNA decay have yet to be comprehensively addressed. Identification of P-bodies might provide information on how mRNA degradation machineries evolved in lower eukaryotes. Here, we used immunofluorescence and confocal microscopy assays to investigate the cellular localization of mRNA degradation proteins in the human intestinal parasite *Entamoeba histolytica* and found evidence of the existence of P-bodies. Two mRNA decay factors, namely the *EhXRN2* exoribonuclease and the *EhDCP2* decapping enzyme, were localized in cytoplasmic foci in a pattern resembling P-body organization. Given that amoebic foci appear to be smaller and less rounded than those described in higher eukaryotes, we have named them “P-body-like structures”. These foci contain additional mRNA degradation factors, including the *EhCAF1* deadenylase and the *EhAGO2-2* protein involved in RNA interference. Biochemical analysis revealed that *EhCAF1* co-immunoprecipitated with *EhXRN2* but not with *EhDCP2* or *EhAGO2-2*, thus linking deadenylation to 5'-to-3' mRNA decay. The number of *EhCAF1*-containing foci significantly decreased after inhibition of transcription and translation with actinomycin D and cycloheximide, respectively. Furthermore, results of RNA-FISH assays showed that (i) *EhCAF1* colocalized with poly(A)⁺ RNA and (ii) during silencing of the *Ehpc4* gene by RNA interference, *EhAGO2-2* colocalized with small interfering RNAs in cytoplasmic foci. Our observation of decapping, deadenylation and RNA interference proteins within P-body-like foci suggests that these structures have been conserved after originating in the early evolution of eukaryotic lineages. To the best of our knowledge, this is the first study to report on the localization of mRNA decay proteins within P-body-like structures in *E. histolytica*. Our findings should open up opportunities for deciphering the mechanisms of mRNA degradation and RNA-based gene silencing in this deep-branching eukaryote.

Citation: López-Rosas I, Orozco E, Marchat LA, García-Rivera G, Guillen N, et al. (2012) mRNA Decay Proteins Are Targeted to poly(A)⁺ RNA and dsRNA-Containing Cytoplasmic Foci That Resemble P-Bodies in *Entamoeba histolytica*. PLoS ONE 7(9): e45966. doi:10.1371/journal.pone.0045966

Editor: Georg Stoecklin, German Cancer Research Center, Germany

Received: April 4, 2012; **Accepted:** August 23, 2012; **Published:** September 24, 2012

Copyright: © 2012 López-Rosas et al. This is an open-access article distributed under the terms of the Creative Commons Attribution License, which permits unrestricted use, distribution, and reproduction in any medium, provided the original author and source are credited.

Funding: This work was supported by Mexico-France (SEP-CONACYT-ANUIES; ECOS NORD) grant M08-S02 and European community grants. The authors acknowledge Autonomous University of Mexico City for support. The funders had no role in study design, data collection and analysis, decision to publish, or preparation of the manuscript.

Competing Interests: The authors have declared that no competing interests exist.

* E-mail: cesar.lopez@uacm.edu.mx

Introduction

The control of messenger RNA (mRNA) degradation plays a key role in the posttranscriptional regulation of gene expression [1]. In eukaryotic cells, mRNA degradation is initiated by shortening of the 3' end-poly(A)⁺ tail by the CCR4/CAF1/NOT1–5 complex and the PAN2, PAN3 and PARN deadenylases [2]. Next, the DCP1 and DCP2 decapping enzymes remove the cap from the 5' end of the deadenylated mRNA in a process stimulated by Dhh1, Edc3, Pat1/Mrt1, Sm-like (Lsm1p–7p) and Hedls proteins [3]. Lastly, the uncapped mRNA body is degraded by XRN1 and XRN2 exoribonucleases in the 5'-to-3' direction.

Alternatively, mRNA is degraded in the 3'-to-5' direction by a complex of PH-like ribonucleases known as the exosome [4].

There is growing body of evidence to show that mRNA degradation occurs in specialized cytoplasmic foci variously referred to as mRNP granules, mRNA-decay foci, GW182-bodies and mRNA processing bodies (P-bodies). These structures are enriched in RNA substrates and mRNA turnover proteins. P-bodies are mRNA processing centers within which non-translating transcripts are sorted and either silenced or degraded [5]. Although the protein inventory of P-bodies has not been defined in detail, around 25 different factors have been detected within these small cytoplasmic domains [6]. The P-bodies observed in

yeast, insect, nematode and mammalian cells have critical roles in mRNA degradation, mRNA storage, mRNA surveillance and RNA-based gene silencing mechanisms [7]. In fact, it has been demonstrated that P-bodies have high concentration of target transcripts and the AGO2, DICER, and GW182 proteins involved in RNA interference by microRNAs (miRNAs) and small interfering RNAs (siRNAs) [8,9,10]. In addition, P-bodies also contain the UPF and SMG families of proteins involved in the nonsense mediated decay (NMD) mechanism that degrades aberrant mRNAs containing premature translation termination codons. [11]. In mammals, most cells contain from three to nine P-bodies, although this number appears to depend on the cell's proliferation ratio and stress conditions, such as nutrient deprivation, oxidative stress and heat shock. Cell treatments with inhibitors of transcription or translation (such as actinomycin D and cycloheximide, respectively) lead to the disassembly of P-bodies [12]. In contrast, treatment with puromycin increases the number and size of P-bodies; this observation emphasizes the relevance of active mRNA and protein synthesis in the assembly of these structures [10]. Even though P-body components clearly play crucial roles in mRNA degradation, there is also evidence to show that NMD and silencing mediated by miRNAs and siRNAs occur in cells lacking detectable P-bodies. This suggests that P-body formation is a consequence, rather than a cause, of mRNA degradation activity [10,13]. Furthermore, translational repression by miRNAs does not require P-body structures; the localization of miRNAs and RNA-induced silencing complex (RISC) proteins within P-bodies appears to be a consequence of translational repression [14].

Human amebiasis is caused by infection with the intestinal protozoan parasite *Entamoeba histolytica*. The disease is endemic in many developing countries and affects around 50 million people worldwide [15]. The symptoms of amebiasis include colitis, dysentery and extra-intestinal abscesses. Despite the importance of post-transcriptional events in the regulation of gene expression, the parasite's mRNA degradation and RNA-based gene silencing mechanisms are poorly understood. Some proteins involved in the RNA interference pathway, including *Eh*AGO2-2, *Eh*RNAseIII and *Eh*RdRP, have been identified and characterized in *E. histolytica* [16,17]. However, proteins involved in mRNA decay pathways have not previously been studied and the potential role of P-bodies in mRNA decay and RNA interference has not been clearly established in protozoan parasites. Here, we sought to localize mRNA degradation factors within *E. histolytica* and found evidence of the existence of P-body-like structures. Our findings open up opportunities for deciphering the mechanisms of mRNA decay and RNA gene silencing in this parasitic, deep-branching eukaryote.

Results

mRNA degradation machineries in *Entamoeba histolytica*

In order to identify homologous genes potentially involved in mRNA decay in *E. histolytica*, we screened the parasite genome at AmoebaDB (<http://amoebadb.org/amoeba/>) by using the amino acid sequences of yeast and human proteins involved in mRNA turnover as probes. Heuristic searches identified several putative protein-encoding genes for mRNA degradation machineries, including deadenylation, decapping, NMD, and RNA interference activities (Figure 1, Table S1). Our data indicated that although several important genes are lacking, mRNA decay machineries are generally well conserved in *E. histolytica*. We detected putative *Ehdcp2*, *Ehlsm1-6*, *Ehedc3* and *Ehdhh1* genes (coding for mRNA decapping factors) and an *Ehxm2* gene (coding for a putative 5'-to-

3' exoribonuclease). In contrast, we did not find any *dcp1* or *xm1* homologs. We also identified genes for NOT1–5 subunits and for *Eh*CAF1 and *Eh*CAF1-like deadenylases. In contrast, the lack of a *ccr4* deadenylase homolog suggested the existence of a CAF1/NOT complex lacking one of the major deadenylases. Intriguingly, we did not detect *pan2*, *pan3* and *pan* genes; this indicates that *E. histolytica*'s deadenylation machinery is smaller than those described in yeast and in the human. Amoeba genome also contains genes for the NMD machinery, as represented by three *Ehufp* genes (Table S1). RNA interference pathway members, including *Eh*RdRP, *Eh*RNAseIII and *Eh*AGO2-2 proteins, have already been reported in this parasite [16,17]. We (like others) did not detect DICER and GW182 homologs, suggesting that RNA interference may occur by small interfering RNAs generated by DICER-independent mechanisms in *E. histolytica* [18].

mRNA degradation genes are differentially expressed under diverse stress conditions

We next sought to establish whether mRNA degradation genes are transcribed in *E. histolytica* trophozoites grown in basal culture conditions and how these genes are modulated in response to the stress induced by heat shock, UV-C-induced DNA damage and nitric oxide treatments, as described elsewhere [19,20,21]. We designed specific primers (Table S2) and performed quantitative real time-PCR assays for representative genes from the various mRNA degradation machineries (Figure 2). After heat shock, *Ehxm2*, *Ehlsm1*, *Ehufp1*, and *Ehmase III* gene expression was found to be upregulated 1.5- to 12-fold relative to non-treated cells, whereas the *Ehcaf1*, *Ehnot1*, *Ehdcp2* and *Ehago2-2* genes were repressed 2-fold (Figure 2). After UV-C-induced DNA damage, *Ehufp1* was upregulated by a factor of 6, whereas the expression of *Ehcaf1*, *Ehnot1*, *Ehdcp2*, *Ehlsm1*, *Ehedc3* and *Ehmase III* genes was significantly repressed. *Ehxm2* and *Ehago2-2* mRNA levels were similar in treated and non-treated cells. *Ehnot1* and *Ehdcp2* genes were significantly repressed after exposure to nitrosative stress in comparison with untreated trophozoites, whereas *Ehcaf1*, *Ehlsm1*, *Ehufp1*, *Ehago2-2* and *Ehmase III* were upregulated 2- to 16-fold. We quantified the mRNA expression of the L31 ribosomal protein-encoding gene as an endogenous control; its expression did not change significantly under any of the tested stress conditions.

*Eh*XRN2 and *Eh*DCP2 have the typical architecture of a 5'-3' exoribonuclease and a decapping protein, respectively

To initiate the study of mRNA degradation proteins in *E. histolytica*, we focused on the putative *Eh*XRN2 exoribonuclease and the *Eh*DCP2 decapping enzyme. We selected these proteins because their homologs have been described as P-body markers in the human and in yeast [22]. Homologous XRN2 and DCP2 proteins from a variety organisms were assigned by BLAST analysis and ClustalW multi-alignments of predicted amino acid sequences (Figure S1A, S2A, and Table S3, S4). *Ehxm2* is an intronless gene (2813 nt) that predicts a 938 amino acids polypeptide. Sequence similarity searches revealed that *Eh*XRN2 exhibits 46% identity ($e = 4.9e-139$) and 45% identity ($e = 1.2e-108$) with *Homo sapiens* XRN2 and *Schizosaccharomyces pombe* RAT1, respectively. Phylogenetic inference of full-length XRN2 sequences revealed that *Eh*XRN2 is closely related to homologous proteins from other protozoa (Figure S1B). Comparison of the amino acids sequence of *Eh*XRN2 with those of *Hs*XRN2 and *Sp*RAT1 homologs indicate the presence of conserved functional and structural motifs as represented by the XRN_N nuclease domain and the internal tower domain (Figure 3A), which is responsible for catalytic activity in *Sp*RAT1 [23]. Importantly, the active site

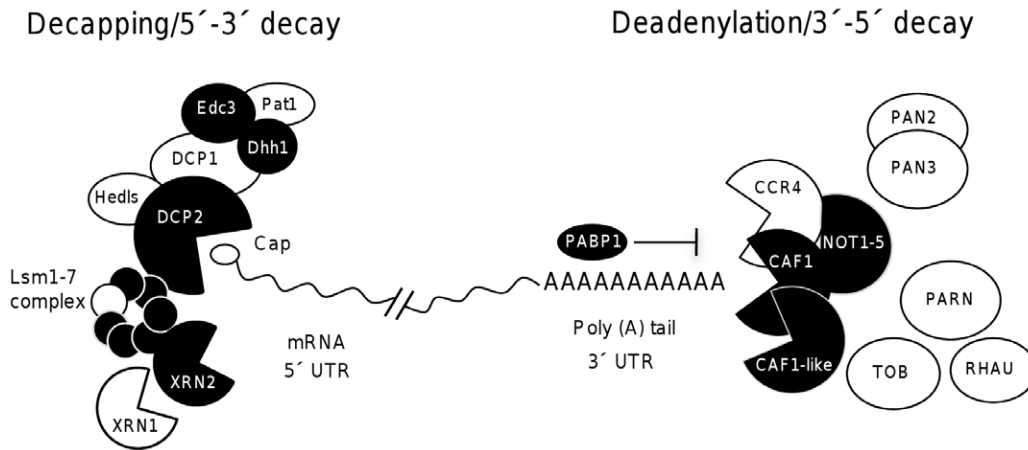


Figure 1. A comparative representation of mRNA decay machineries in *E. histolytica* (black shapes) and *H. sapiens* (white and black shapes). Homologous proteins were assigned via BLAST and ClustalW multiple alignments. The undulated line denotes mRNA. doi:10.1371/journal.pone.0045966.g001

motif KX_2QQX_2RR , which is critical for *SpRAT1* ribonuclease function, is well conserved in *EhXRN2*. The high degree of homology between *EhXRN2* and *SpRAT1* allowed us to construct a structural model of *EhXRN2* by using *SpRAT1* crystal data as template. The predicted tertiary structure suggested that the *EhXRN2* N-terminal domain is constituted by a six α -helix bundle and a two-stranded β -sheet, the orientation and length of which is similar to that found in the *SpRAT1* structural model (Figure 3B–C).

The *Ehdcp2* gene (699 nt) contains two introns and predicts an open reading frame of 233 amino acids. *EhDcp2* exhibits 28% ($e = 8.4e-25$) and 29% ($e = 1.6e-19$) identity with human DCP2 and yeast DCP2, respectively. Phylogenetic inference revealed that

EhDcp2 is closely related to homologous proteins from other protozoa (Figure S2B). *EhDcp2* contains the conserved DCP2 box A domain (Figure 3D) and the consensus sequence for the nudix motif $GX_5EX_7REUXEEXGU$ (including the three catalytic glutamate (E) residues). In mammalian cells, both these domains are responsible for cap structure removal [24]. Modeling of *EhDcp2*'s tertiary structure using the *ScDcp2* structure as a template indicated that the two proteins are similar in terms of conformation and length (Figure 3E–F).

EhXRN2, *EhDcp2* and *EhCAF1* are cytoplasmic proteins

We next investigated the cellular localization of *EhXRN2* and *EhDcp2* factors in *E. histolytica*. An *Ehxm2* gene fragment (351 nt)

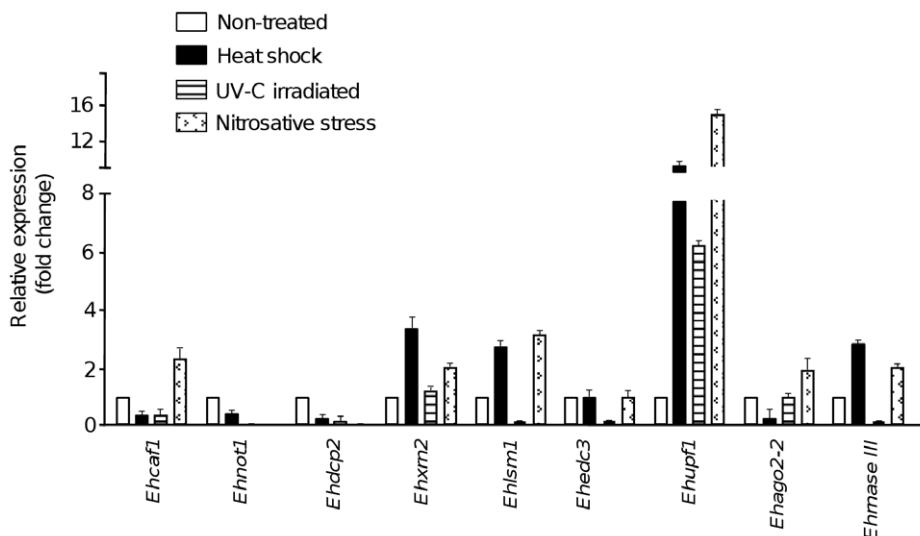


Figure 2. mRNA expression profiles of genes for *E. histolytica* mRNA degradation proteins. Quantitative real-time PCR assays were performed to analyze the relative expression of representative mRNA degradation genes after heat shock, UV-C induced DNA damage and sodium nitroprusside treatments. For each triplicate experiment, the mean of the relative concentrations obtained for the tested mRNA were divided by the mean of the corresponding values obtained for endogenous ribosomal *L31* amplification. Each PCR experiment was carried out three times and three independent biological samples were analyzed. The relative expression (fold change) of mRNA degradation genes in the different treatments was calculated by the $2(-\Delta\Delta Ct)$ method using as reference the Ct data for the untreated condition. Bars indicate the mean \pm SD. doi:10.1371/journal.pone.0045966.g002

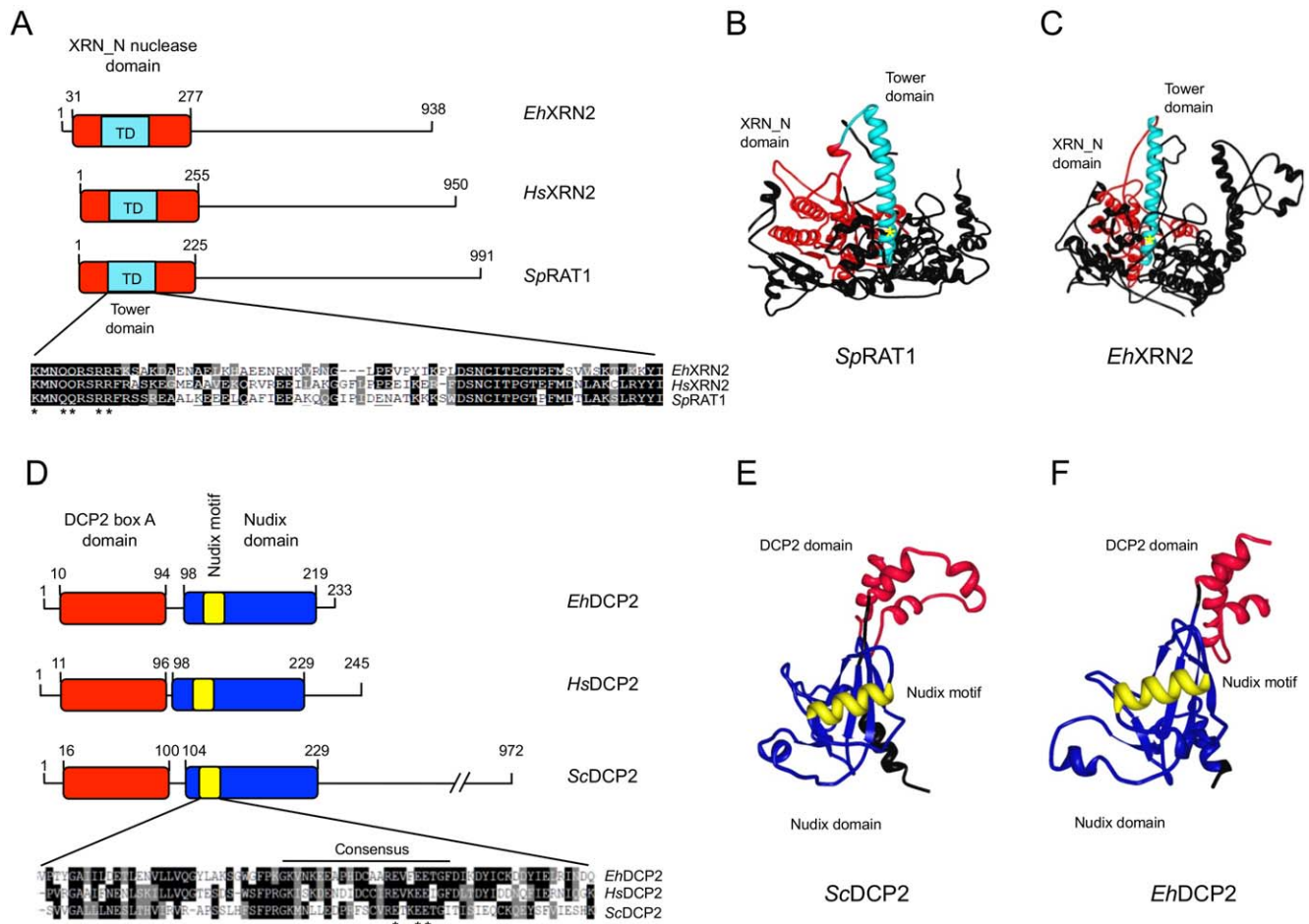


Figure 3. Comparison of XRN2 and DCP2 from eukaryotic organisms and *E. histolytica*. (A) A schematic representation of XRN2 protein from *E. histolytica*, *H. sapiens* and *S. pombe*. Red box: the XRN domain; cyan box: the tower domain (TD). The numbers are relative to the initial methionine in each protein. Lower panel: multiple alignments of amino acid residues from the TD of homologous proteins. Black box: a conserved residue; grey box: a conserved substitution. Asterisks mark the conserved residues in the active site. (B, C) Ribbon diagrams of ScRAT1's tertiary structure (B) and the predicted model of *EhXRN2* (C). Red: the N-terminal XRN_N domain; cyan: the TD. (D) A schematic representation of the DCP2 protein from *E. histolytica*, *H. sapiens*, and *S. cerevisiae*. Red box: the DCP2 domain; blue box: the nudix domain. The numbers are relative to the initial methionine in each protein. Lower panel: multiple alignments of amino acid residues from the nudix motif (PF00293) of homologous proteins. Asterisks indicate the conserved residues involved in catalytic activity. Black box: a conserved residue; grey box: a conserved substitution. (E, F) Ribbon diagrams of ScDCP2's tertiary structure (E) and the predicted model of *EhDCP2* (F). Red: the DCP2 domain; blue: the nudix domain; yellow: the nudix motif. Three-dimensional models were displayed and refined using the RCSB PDB Protein Workshop 3.9 viewer.
doi:10.1371/journal.pone.0045966.g003

and the full-length *Ehdcp2* gene were PCR-amplified from genomic DNA and cloned in-frame into the pRSET-A expression vector. Recombinant 6xHis-tagged *EhXRN2* and *EhDCP2* polypeptides were expressed in bacteria (Figure 4A and B; lane 2), purified by affinity chromatography and used as immunogens in the mouse to obtain specific antibodies. In Western blot assays based on anti-*EhXRN2* and *EhDCP2* antibodies, we detected the corresponding purified recombinant proteins (Figure 4A and B, lane 5). The subcellular localization of *EhXRN2* and *EhDCP2* were investigated by Western blotting cytoplasmic and nuclear protein extracts from *E. histolytica* trophozoites (Figure 4C). In the cytoplasmic fraction, specific antibodies recognized bands at 103 kDa and 27.5 kDa, which correspond to the predicted molecular weights for endogenous *EhXRN2* and *EhDCP2* proteins, respectively (Figure 4C, lanes 2 and 4). In contrast, no proteins in the nuclear fraction (lanes 1 and 3) were recognized. The results of control assays with used pre-immune serum (which did not give any signal;

data not shown) and antibodies that recognized the *EhPC4* transcription factor (found mainly in the nuclear fraction (lane 5), as reported elsewhere [25]) confirmed the absence of cross-contamination between cytoplasmic and nuclear fractions.

We then used immunofluorescence and confocal microscopy assays to study the distribution of mRNA degradation proteins within trophozoites. As shown in Figure 4, *EhXRN2* and *EhDCP2* proteins were diffusely immunodetected throughout the cell (D-H and I-M) but were mainly concentrated in bright cytoplasmic foci with a diameter ranging from 50 to 300 nm; this resembled the organization into P-bodies seen in higher eukaryotes. To further investigate the localization of additional mRNA degradation proteins within trophozoites, we studied the cellular distribution of *EhCAF1* deadenylase using specific rabbit antibodies generated in-house (manuscript in preparation). In particular, *EhCAF1* had a similar pattern to *EhXRN2* and *EhDCP2* within cytoplasmic foci and a more diffuse general staining (Figure 4N-R).

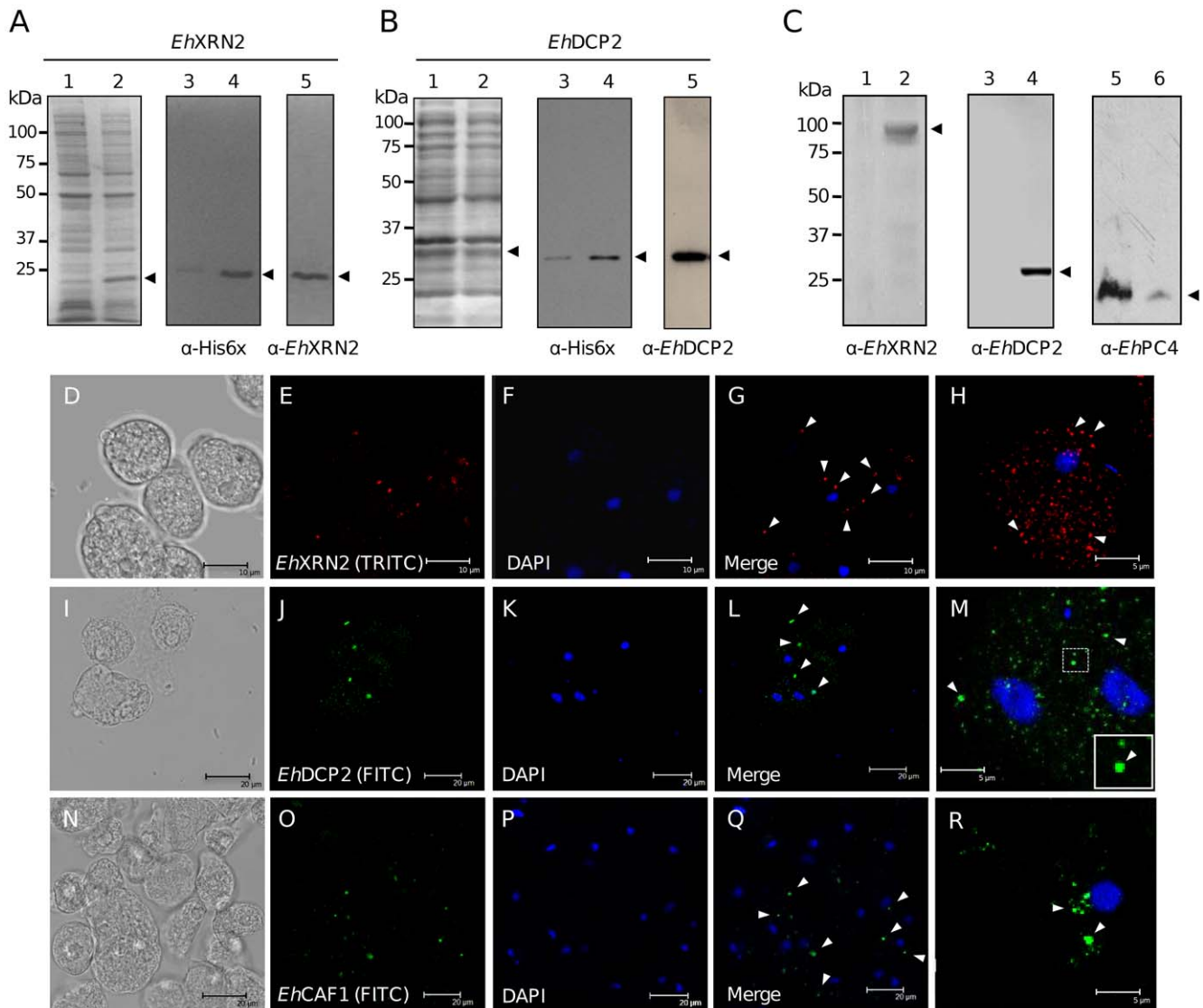


Figure 4. Expression and immunolocalization of *EhXRN2*, *EhDCP2* and *EhCAF1*. (A–B) Expression of 6xHis-tagged *EhXRN2* (A) and *EhDCP2* (B) proteins. Bacterial proteins were separated by 12% SDS-PAGE and the gels were stained with Coomassie blue. Lane 1: non-induced bacterial extracts; lane 2: IPTG-induced bacterial extracts. Western blot assays were performed using anti-6xHis tag antibodies and non-induced bacterial extracts (lane 3) or IPTG-induced bacterial extracts (lane 4). Recombinant *EhXRN2* and *EhDCP2* proteins were also immunodetected with specific antibodies (lane 5). (C) Immunodetection of *EhXRN2* (lanes 1 and 2), *EhDCP2* (lanes 3 and 4) and *EhPC4* (lanes 5 and 6) proteins in trophozoites, using specific antibodies. Lanes 1, 3 and 5: nuclear extracts; lanes 2, 4 and 6: cytoplasmic extracts. (D–R) Confocal immunofluorescence microscopy assays for the localization of *EhXRN2* (E), *EhDCP2* (J) and *EhCAF1* (O) in fixed trophozoites using FITC-antibodies. Middle panels (F, K, P) show nuclear staining with DAPI and right-hand panels (G, L, Q) show overlays of the two signals. Different magnifications of single cells were used to enhance the visibility of cytoplasmic structures (H, M, R). Arrowheads indicated some typical foci.
doi:10.1371/journal.pone.0045966.g004

EhXRN2, *EhDCP2* and *EhAGO2-2* colocalize within *EhCAF1*-containing cytoplasmic foci

The observed colocalization of *EhXRN2*, *EhDCP2* and *EhCAF1* prompted us to look for common focal, cytoplasmic structures. We performed co-immunolocalization and confocal microscopy assays in trophozoites by using *EhCAF1* as a marker for the P-body-like structures (Figure 5). Our data showed that both *EhXRN2* and *EhDCP2* co-immunolocalized within the majority of *EhCAF1*-containing-cytoplasmic foci (Figure 5, A–D and E–H). We next wondered whether additional factors related to mRNA degradation might also accumulate with *EhXRN2* and *EhDCP2* in a unique set of *EhCAF1*-containing foci. Hence, we performed immunofluorescence experiments using antibodies

raised against *EhAGO2-2* an Argonaut protein involved in RNA interference [18]. Indeed, the *EhAGO2-2* signal also colocalized with *EhCAF1* in trophozoites (Figure 5, I–L). None of these proteins gave a significant nuclear signal. Taken as a whole, our data indicate that these mRNA degradation factors are concentrated within cytoplasmic P-body-like structures.

We next sought to establish whether the colocalized *EhXRN2*, *EhDCP2*, *EhCAF1*, and *EhAGO2-2* proteins could interact physically by performing co-immunoprecipitation assays with anti-*EhCAF1* or -*EhXRN2* antibodies as bait and trophozoite cytoplasmic proteins as prey (Figure 5M). Our results showed that *EhCAF1* co-immunoprecipitated with *EhXRN2* and *vice versa*; these data fit with the co-immunolocalization studies and suggest a

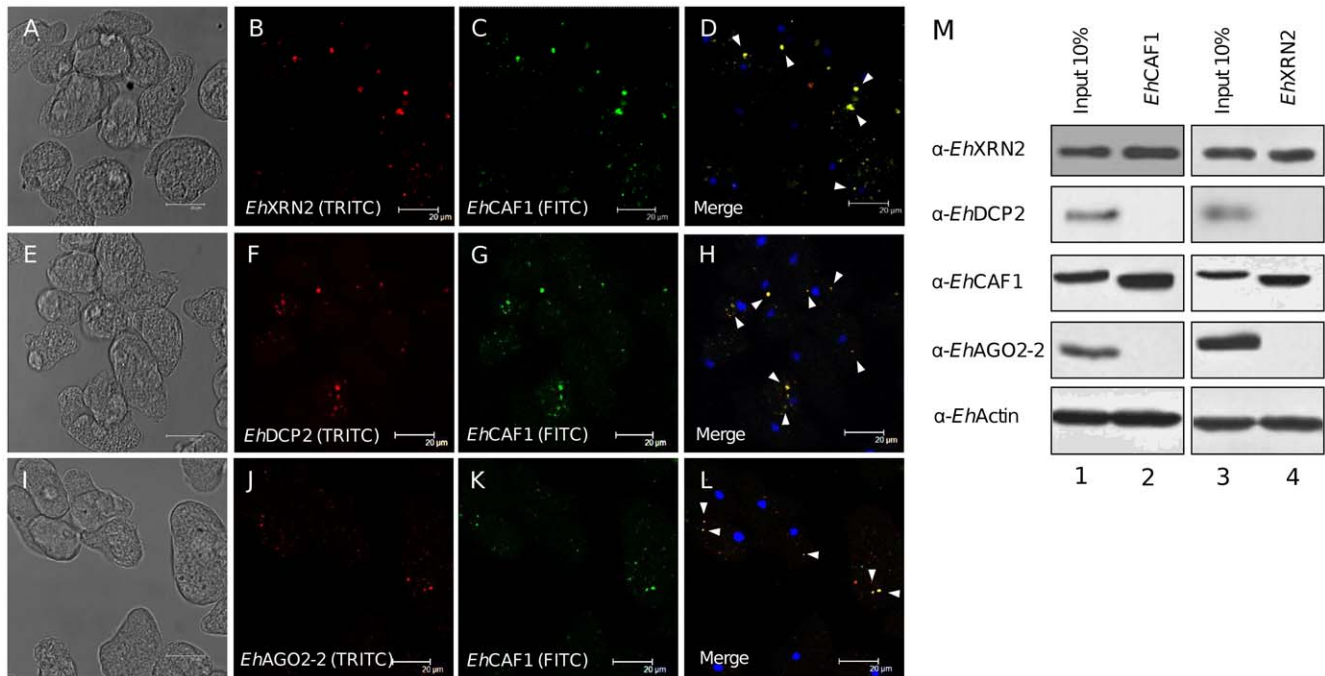


Figure 5. Colocalization of mRNA decay factors with *EhCAF1* in cytoplasmic foci. (A–L) Confocal immunofluorescence microscopy assays. Trophozoites were incubated with anti-*EhXRN2* (B), anti-*EhDCP2* (F), anti-*EhAGO2-2* (J) and anti-*EhCAF1* (C, G, K) primary antibodies (1:100). Secondary antibodies included TRITC-conjugated anti-mouse IgG (1:200) and FITC-conjugated anti-rabbit IgG (1:200). (A, E and I): light microscopy; (B, F and J): the red channel; (C, G and K): the green channel; (D, H and L): merged images. Arrowheads mark typical, colocalized signals in cytoplasmic foci. (M) Immunoprecipitation assays using anti-*EhCAF1* and anti-*EhXRN2* antibodies conjugated to protein G beads with cytoplasmic lysates of *E. histolytica* trophozoites. Immunoprecipitates were separated with SDS-PAGE and analyzed by Western blotting with the antibodies indicated at the left side of each panel. Lanes 1 and 3: input (10% of the total lysate used for immunoprecipitation); lanes 2 and 4: immunoprecipitated proteins. doi:10.1371/journal.pone.0045966.g005

novel functional link between deadenylation and 5'-to-3' mRNA degradation (Figure 5M, upper panel, lanes 2 and 4). In contrast, we did not detect co-immunoprecipitation of *EhCAF1* with either *EhDCP2* or *EhAGO2-2* - suggesting that despite their colocalization in cytoplasmic foci in trophozoites, these proteins do not interact. Surprisingly, we also found co-immunoprecipitation of actin protein with both baits (Figure 5M, bottom panel, lanes 2 and 4). In agreement with these results, we also identified actin as an *EhCAF1*-interacting protein in pull-down assays using GST-*EhCAF1* recombinant fusion protein as bait and cytoplasmic proteins as prey (manuscript in preparation). It has been reported that mammalian P-body proteins are anchored to the cytoskeleton and associate with tubulin and actin-bundles in human cells, suggesting that P-bodies require a dynamic interaction with the cytoskeleton [26].

The formation of cytoplasmic foci depends on the presence of active transcription

To evaluate the impact of active ongoing transcription on P-body size and number, we measured the change over time in the number of *EhCAF1*-containing foci after transcription inhibition with actinomycin D, as described elsewhere [27]. Our results showed that abrogation of transcription considerably altered the number of cytoplasmic foci (Figure 6A). We observed that number of cytoplasmic foci per cell diminished significantly after 4 h of incubation with actinomycin D. After 12 h treatment, the number of foci per cell had fallen by 50%. This effect was not observed in cells treated with the vehicle DMSO alone. The results of Western blot assays showed that the expression level of *EhCAF1* was not significantly affected by actinomycin D treatment (data not

shown). Hence, the fall in the number of foci was not due to the inhibition of *EhCAF1* expression. Our data indicate that cytoplasmic foci formation is linked to active transcription – a feature that is conserved in P-bodies in higher eukaryotes.

Inhibition of translation affects cytoplasmic foci formation

A common feature of mammalian P-bodies is that they are disrupted by drugs such as cycloheximide that stabilize mRNAs in polysomes, whereas their number and size are increased by drugs such as puromycin that release ribosomes from mRNA [10,12]. To evaluate the effect of inhibiting protein synthesis on the number and size of *EhCAF1*-containing cytoplasmic foci, we treated *E. histolytica* trophozoites with cycloheximide or puromycin. The results showed that the number of foci per cell rapidly fell after 15 min of incubation with cycloheximide and almost disappear after 120 min of treatment (Figure 6B). In contrast, puromycin treatment led to a slight increase in the number of cytoplasmic foci after 120 min (Figure 6C). Control assays showed that DMSO alone did not have a significant effect on the number of *EhCAF1*-containing foci.

EhCAF1 and *EhAGO2-2* colocalize with poly(A)⁺ RNA and dsRNA substrates

We next looked at whether polyadenylated RNA substrates accumulate in P-body-like foci under basal culture conditions. Poly(A)⁺ RNAs were detected in trophozoites by fluorescence *in situ* hybridization (FISH) with a FITC-labeled oligo(dT)₃₀ probe. *EhCAF1* foci were evidenced by immunofluorescence with specific antibodies. Interestingly, our results showed that although

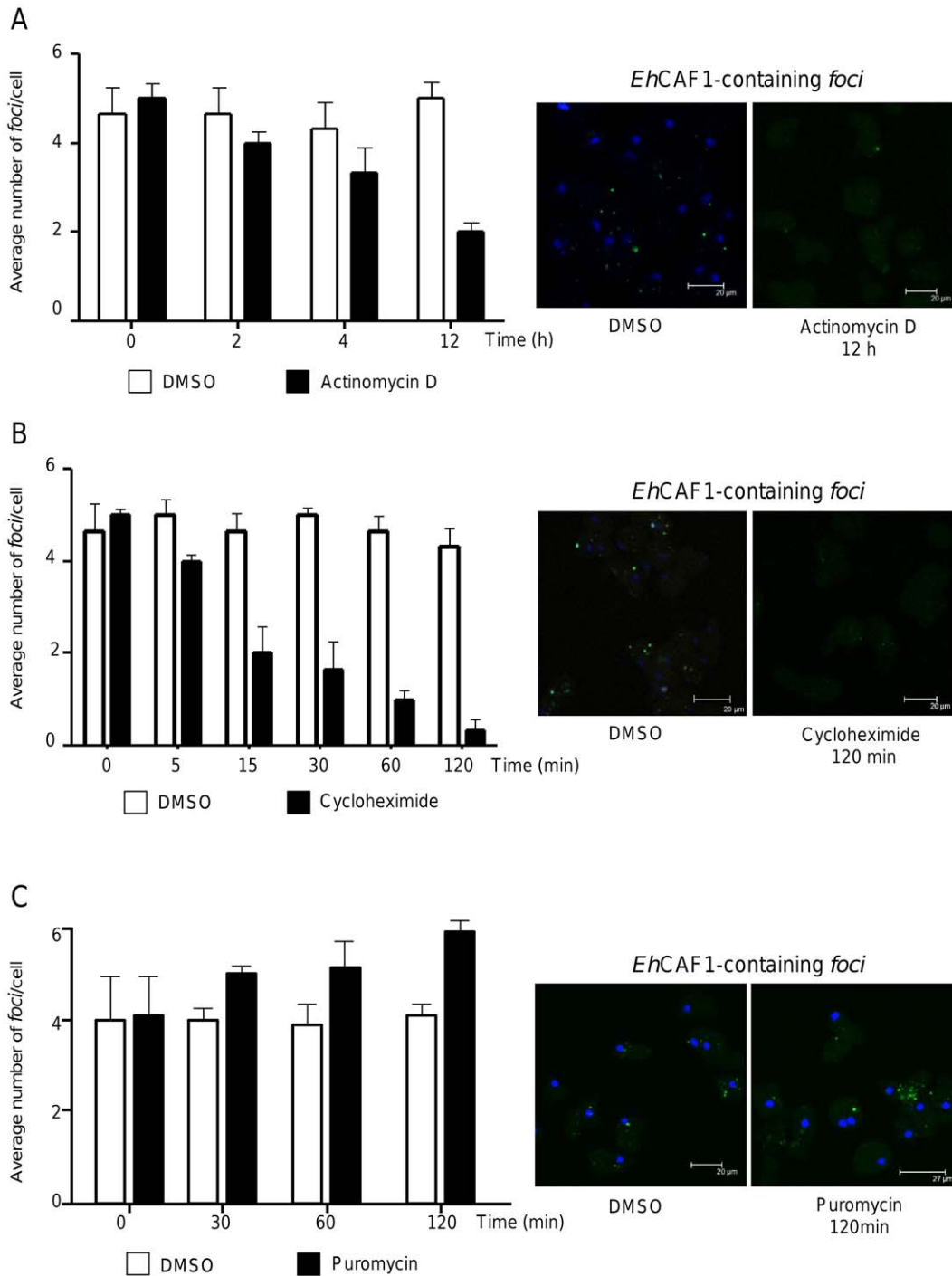


Figure 6. Determination of the number of *EhCAF1*-containing cytoplasmic foci after treatment with actinomycin D, cycloheximide or puromycin. After treatment with actinomycin D (5 $\mu\text{g/ml}$, panel A), cycloheximide (10 $\mu\text{g/ml}$, panel B) or puromycin (200 $\mu\text{g/ml}$, panel C), trophozoites were fixed, incubated with anti-*EhCAF1* and FITC-labeled secondary antibodies, counterstained with DAPI and analyzed under an immunofluorescence confocal microscope. Left panel: change over time in the mean number of foci per trophozoite, in response to inhibition of transcription (A) or translation (B–C). The data correspond to six randomly chosen fields. Right panel: representative images of cells treated with DMSO vehicle (control) and actinomycin D, cycloheximide or puromycin (observed in the green channel).
doi:10.1371/journal.pone.0045966.g006

the FITC-oligo(dT)₃₀ signal was dispersed throughout the cytoplasm, a small proportion of probe colocalized with immunostained *EhCAF1* in cytoplasmic foci (Figure 7E). Control experiments showed that the FITC-oligo(dT)₃₀ signal was specific

for RNA, since it disappeared after RNase A treatment (Figure 7F–J).

To gain insights into the potential role of P-body-like structures in RNA interference, we sought to determine whether a specific double-stranded RNA (dsRNA) accumulated in cytoplasmic foci

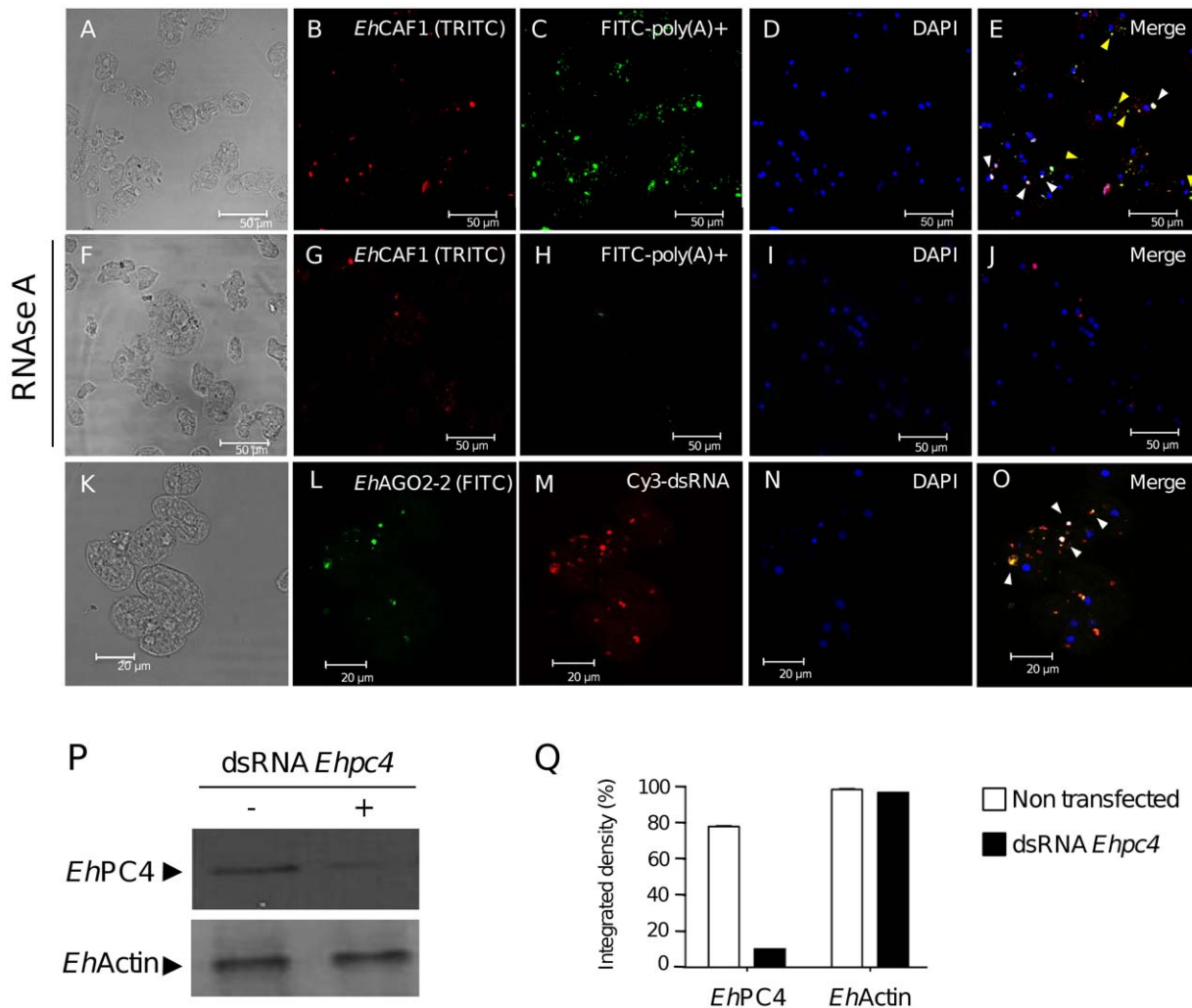


Figure 7. Colocalization of poly(A)⁺ RNA and dsRNA substrates with *EhCAF1* and *EhAGO2-2* in cytoplasmic foci. (A–E) Poly(A)⁺ RNA and *EhCAF1* colocalization assays. Trophozoites were immunostained with *EhCAF1* (B) antibodies. Poly(A)⁺ RNAs were detected by hybridization with FITC-conjugated oligo-(dT)₃₀ (C). The cells were counterstained with DAPI (D) and analyzed with immunofluorescence confocal microscopy. The merged image (E) shows the overlapping signals. White arrowheads indicate the accumulation of poly(A)⁺ RNA and *EhCAF1* signals. Yellow arrowheads indicate FITC-poly(A)⁺ signal that does not overlap with *EhCAF1*-containing foci. (F–J) RNase A treatment, performed as a control experiment. Immunodetection of *EhCAF1* (G), detection of poly(A)⁺ (H) and DNA counterstaining with DAPI (I). Merged image (J). (K–O) *EhAGO2-2* and Cy3-dsRNA colocalization assays. Trophozoites were transfected with Cy3-dsRNA targeting *Ehpc4* (K–O) and then immunostained with *EhAGO2-2* antibodies on day seven after transfection (L). Cells were counterstained with DAPI (N) and analyzed with immunofluorescence confocal microscopy. The merged image (O) shows both signals. Arrowheads mark colocalized signals in cytoplasmic foci. (P) Western blot analysis for *EhPC4* and *EhActin* from proteins extracts obtained on day seven after Cy3-dsRNA transfection. (Q) A densitometric analysis of the bands in P. doi:10.1371/journal.pone.0045966.g007

and colocalized with *EhAGO2-2* during silencing of an endogenous gene. The long dsRNA was designed to specifically knock down the *Ehpc4* gene expression and its efficacy was validated by using the soaking approach described for amoeba [28]. Briefly, dsRNA was generated in bacteria, purified, Cy3-labeled and transfected into trophozoites to produce fluorescent siRNA. Our data showed that the dsRNA-Cy3 signal was found in discrete, cytoplasmic foci seven days after transfection of the trophozoites (Figure 7M). Moreover, coupled FISH and immunofluorescence assays using the dsRNA-Cy3 probe and *EhAGO2-2* antibodies showed that the two signals colocalized in large, cytoplasmic foci (Figure 7K–O). Remarkably, the focus size and signal intensity for *EhAGO2-2* were greater in cells than in non-transfected, control cells - suggesting that *EhAGO2-2* protein expression was induced by siRNA transfection. Western blot assays confirmed that *EhPC4*

protein levels were reduced by 50% and 80% three and seven days after dsRNA-Cy3 transfection, respectively. This indicated that RNA interference had been successful (Figure 7P–Q). We can rule out the possibility that the cytoplasmic foci containing siRNA against the *Ehpc4* gene were non-transfected vesicles or endosomes, since we used the soaking method to deliver the dsRNA-Cy3 probe to trophozoites. However, we cannot be sure that only the siRNA guide strand was located in the cytoplasmic foci, since it has been reported that siRNAs can localize in P-bodies as dsRNA [29].

Discussion

mRNA decay pathways and machineries have been extensively studied in *S. cerevisiae* and *H. sapiens*. In contrast, little is known about mRNA degradation factors in protozoan parasites. Here, we

identified protein-encoding genes for mRNA degradation machineries in *E. histolytica*. Our identification of decapping, deadenylation, NMD and RNA interference activities suggests that mRNA degradation components and mechanisms are conserved in this parasite. However, the composition of these machineries is simpler than that seen in higher eukaryotic cells - a frequent feature in the small genomes of divergent parasites. Importantly, we found that the deadenylation machinery is incomplete in *E. histolytica* because we did not find *ccr4*, *pan2*, *pan3*, or *pam* deadenylases; this result suggests that *EhCAF1* is the parasite's main poly(A) ribonuclease. Furthermore, the decapping machinery lacks *dcp1* and *xrn1* genes but contains DCP2 and XRN2 homologs, which are typical P-body markers. Interestingly, the *EhXRN2* and *EhDCP2* proteins involved in 5'-to-3' mRNA decay accumulated in discrete cytoplasmic foci in a manner similar to that seen in P-bodies in higher eukaryotes. This localization pattern was also observed for *EhCAF1* deadenylase and *EhAGO2-2*. Given that DCP2, XRN2, CAF1 and AGO2 are resident P-body proteins in human cells, our data suggest that the foci observed in *E. histolytica* correspond to P-bodies. However, the amebic foci are smaller and less rounded than P-bodies and so we prefer to refer to them as P-body-like structures. Given the similarity between proteins involved in mRNA decay in the human, in yeast and in *E. histolytica* and the colocalization of *EhCAF1* with *EhXRN2* and *EhAGO2-2* in cytoplasmic structures, our results also suggest that mRNA degradation occurs at these foci. However, this hypothesis requires formal confirmation through additional experiments designed to evidence the degradation of RNA substrates and the localization of other mRNA decay proteins in these P-body-like structures.

Cytoplasmic foci resembling P-bodies have previously been described in the protozoan parasite *Trypanosoma*. Cassola *et al.* [30] reported that mRNA and proteins related to mRNA metabolism were concentrated in cytoplasmic mRNA granules in starved *T. cruzi* and *T. brucei* parasites and suggested that the said granules provided transient protection of transcription during periods of stress. However, these structures may not represent typical P-bodies. A complex containing CAF1, NOT1, NOT2, NOT5, DHH1 and a possible homolog of Caf130 was found in *T. brucei*, in which CAF1 deadenylation activity was shown to be essential for cell survival [31]. In particular, CAF1 protein appeared to be predominantly distributed in the cytoplasm and the characteristic, punctate staining indicative of association with RNA storage or degradation granules was not found. Holetz *et al.* [32] showed that the Tcdhh1 helicase protein was present in polysome-independent complexes and in discrete cytoplasmic foci resembling P-bodies. The latter varied in number as a function of the cell's nutritional status and following cycloheximide and puromycin treatments. Despite these initial efforts, the existence and potential roles of P-bodies in mRNA degradation events in protozoan parasites have not been comprehensively addressed.

We cannot rule out the existence of other RNA-containing foci in *E. histolytica*, such as the stress granules described in eukaryotic cells. Stress granules are cytoplasmic aggregates of stalled 48S pre-initiation complexes. They include small ribosomal subunits, translation initiation factors (eIF2, eIF3, eIF4, eIF4G), PABP, p54/Rck and the TTP and CPEB RNA binding proteins that regulate mRNA translation and decay [33,34]. Although P-bodies and stress granules share some proteins (e.g. TTP, p54/Rck, Lsm1, and Xrn1), there are some notable differences; P-bodies contain components of the mRNA decay pathway, whereas stress granules contain components of the translation initiation machinery and other specific markers (including TIA1) [35,36]. The presence of stress granules in *E. histolytica* remains to be established;

studies with specific markers would be required to gain a comprehensive view of cytoplasmic structures containing RNA binding proteins in this parasite.

In mammalian cells, treatment with actinomycin D induces the loss of P bodies [12], suggesting that the latter disaggregate once mRNA transcripts are no longer available for degradation. In contrast, the fact that trypanosome mRNA granules persist after actinomycin D treatment suggests that transcript degradation does not take place in these structures [30]. P-body formation in human and yeast also depends on the presence of elevated levels of non-translating mRNAs, which indicates that mRNAs exit the translation cycle before they enter P-bodies [37,38]. The observed effects of transcriptional and translational inhibitors that are known to inhibit mRNA decay suggest that cytoplasmic foci represent sites in which mRNA decay occur. Our data revealed a similar situation in *E. histolytica* trophozoites, since the number of P-body-like structures number fell after treatment with actinomycin D and cycloheximide. It has been reported that the translation inhibitor puromycin induces an increase in the number and size of P-bodies by releasing ribosomes from mRNA. In *E. histolytica* trophozoites, the number of P-body-like structures increase slightly after puromycin treatment. Hence, our data indicate that P-body-like structures are dynamic and are associated with ongoing mRNA synthesis and translation in *E. histolytica*.

The co-immunolocalization of the deadenylase *EhCAF1* and the exoribonuclease *EhXRN2* in cytoplasmic foci in *E. histolytica* supports the hypothesis whereby P-body-like structures have an important role in mRNA decay. Furthermore, these results constitute the first evidence of a functional interaction between deadenylation and 5'-to-3' mRNA degradation. The interaction between actin and both *EhCAF1* and *EhXRN2* further suggests that the proteins in amoebic P-body-like structures are associated with the cytoskeleton, as is the case in the human [26]. Additional, ongoing experiments should help us to understand the implications of these interactions within mRNA degradation machineries.

A small proportion of polyadenylated RNAs was concentrated in cytoplasmic foci, along with *EhCAF1*. In addition, fluorescent siRNAs were rapidly localized with *EhAGO2-2* protein in cytoplasmic foci during RNA interference of *Ehpc4* gene; this observation implies that P-body-like structures may have an important role in siRNA-mediated gene silencing by facilitating the interaction between siRNAs and Argonaut proteins. It was recently reported that *EhAGO2-2* protein was localized in nuclei with siRNAs containing 5'-polyphosphate termini during transcriptional gene silencing in *E. histolytica* strain G3 [39]. Surprisingly, we did not detect a nuclear signal for *EhAGO2-2*. This may be due to the fact that depending on the siRNAs generated during RNA interference, Argonaut proteins can downregulate gene expression by transporting specific classes of small regulatory RNAs to distinct cellular compartments. During transcriptional silencing, *EhAGO2-2* specifically transports small regulatory RNAs to nuclei in which gene silencing is mediated by histone modifications [39]. Our results indicate that both *EhAGO2-2* and specific siRNAs are preferentially targeted to the cytoplasm during RNA interference.

Taken as a whole, our present results provide evidence to suggest that mRNA degradation proteins involved in deadenylation and decapping pathways are organized within cytoplasmic, P-body-like structures that can be observed under the microscope. Future work is needed to understand the composition of these structures and define the localization of other mRNA decay proteins from NMD and RNA interference machineries and thus provide a better understanding of mRNA decay in this protist. This research should also provide us with an opportunity

to answer intriguing, fundamental questions about the posttranscriptional regulation of gene expression in this deep-branching eukaryotic parasite.

Materials and Methods

Ethics statement

This study was carried out in strict accordance with the recommendations of the Guide for the Use of Laboratory Animals of the Investigation Center and Advanced Studies of the National Polytechnic Institute. The protocols and experiments were approved by the Institutional Animal Care of the Investigation Center and Advanced Studies of the National Polytechnic Institute. Animals were kept in environmentally controlled animal facilities at the Investigation Center and Advanced Studies of the National Polytechnic Institute. All surgery was performed under sodium pentobarbital anesthesia and efforts were always made to minimize suffering.

Bacterial strains

Escherichia coli strain BL21pLysS was used for generation of *EhDCP2*, *EhXRN2* and *EhAGO2-2* recombinant proteins. We used the RNase-III deficient *E. coli* strain HT115 (rnc14::VTn10) to generate long dsRNAs targeting the *Ehpc4* gene [40].

E. histolytica cultures

Trophozoites of HM1-IMSS strain were axenically cultured in TYI-S-33 medium [41]. Cells in the logarithmic growth phase were used in all experiments. Cell viability was monitored by microscopy using the trypan blue dye exclusion method.

In silico identification of mRNA degradation genes

Identification of mRNA decay machinery genes was performed by screening the *E. histolytica* genome sequence at AmoebaDB (<http://amoebadb.org/amoeba/>). Human mRNA degradation protein sequences were used as queries. The amino acid sequences of orthologous *E. histolytica* proteins were aligned with those of mRNA degradation proteins from a range of organisms in the UniProt Knowledgebase, using ClustalW software with gap penalties of 10. Structural domains and sequence patterns were predicted with Scan Prosite. Three-dimensional structures for *EhXRN2* and *EhDCP2* were predicted with the SWISS-MODEL program by using the *S. pombe* RAT1 crystal structure (PDB 3FQD) and the *S. cerevisiae* DCP2 crystal structure (PDB 2KQMB) as a template, respectively. Three-dimensional models were displayed and refined using the RCSB Protein Data Bank Protein Workshop 3.9 viewer.

Quantitative real-time PCR assays

Total RNA was obtained using Trizol (Invitrogen) from HM1-IMSS strain trophozoites grown in basal culture conditions and after the induction of cell stress by heat shock, DNA damage and nitric oxide treatment. cDNAs were synthesized using 1 µg total RNA, 100 ng oligo (dT)₁₈, 100 mM DTT, 10 mM dNTPs, 40 U RNase inhibitor (Promega) and 200 U of Superscript II reverse transcriptase (Invitrogen) in first-strand buffer at 42°C for 90 min. After primer-specific reverse transcription, quantitative real-time PCR was performed with the primers listed in Table S2. Three independent biological samples were analyzed.

Quantitative real-time RT-PCR was carried out using an ABI PRISM 7000 Sequence Detection System (Applied BioSystems). Reactions contained 500 nM of each primer, 1× PCR SYBR-Green Master Mix (Qiagen) and 1 µL of template cDNA. Primers used for amplification are listed in Table S2. After an initial

denaturation for 15 min at 95°C, the following amplification cycle (repeated 40 times) was applied: 15 s at 95°C, 15 s at 52°C and 15 s at 72°C. Next, a denaturation curve was established (55°C to 95°C, 2°C min⁻¹) to check that a unique amplicon was produced. For each triplicate, the mean of the relative concentrations obtained for the tested mRNA was divided by the mean of the corresponding values obtained for amplification of the endogenous normalizer ribosomal *L31* gene. This ratio represents the variation of the mRNA abundance in the sample condition, compared with control. Each PCR experiment was repeated three times and three independent biological samples were analyzed. The relative expression of the genes coding for mRNA degradation enzymes was calculated using the 2(-ΔΔCt method) [42].

Expression and purification of recombinant proteins

A 351-base-pair internal region of the *EhXm2* gene (EHI_133330) was PCR-amplified from HM1-IMSS genomic DNA using *Ehxm2-S* (5'-CCGGATCCAGGGAACAACCT-CCTGTA-3') and *Ehxm2-AS* (5'-CCAAGCTTTAACAG-TAGTTGAAAAAACCAC-3') primers. The full-length 699 nt *Ehdcp2* gene (EHI_058810) was PCR-amplified from cDNA using *Ehdcp2-S* (5'-CCCGGATCCATGGATACTCATGTTCCA-3') and *Ehdcp2-AS* (5'-CCAAGCTTTCATCTGGACTTCTT-TATT-3') primers. *Bam*HI and *Hind*III restriction sites are underlined. Amplified PCR products were purified and cloned in-frame into the pRSETA expression vector (Invitrogen). Plasmid constructions were automatically sequenced in an ABI-PRISM 310 sequencer (Applied Biosystems). The *Ehago2-2* gene was subcloned into pRSET-A from the pKT-3M plasmid (generously provided by Dr. Upinder Singh, Stanford University, CA). Recombinant *EhXRN2*, *EhDCP2* and *EhAGO2-2* proteins were expressed as His6x-fusion polypeptides in *E. coli* strain BL21 (DE3) pLysS using 1 mM isopropyl-beta-D-thiogalactopyranoside (IPTG) for 3 hours at 37°C. Cells were disrupted by sonication and soluble *EhXRN2*, *EhDCP2* and *EhAGO2-2* proteins were purified to near-homogeneity under native conditions with Ni-NTA sepharose chromatography (Qiagen). The identity and integrity of recombinant proteins were confirmed by Western blot assays using anti-His6x antibodies (1:10,000) and the ECL-Plus detection system (GE Healthcare).

Generation of antibodies and Western blot assays

After separation by SDS-PAGE, recombinant *EhXRN2*, *EhDCP2* and *EhAGO2-2* proteins were electro-eluted from the Coomassie Blue-stained gel and used to immunize pathogen-free BALB/c male mice (*EhXRN2*, *EhDCP2*) or a rabbit (*EhAGO2-2*) as follows. An initial dose of 20 µg (mice) or 150 µg (rabbit) of recombinant protein in complete Freund's adjuvant (Gibco) was injected subcutaneously inoculated into the animals. Next, three doses of 20 µg (mice) or 100 µg (rabbit) in incomplete Freund's adjuvant (Gibco) were injected via the same route at 21-day intervals. One week after the last immunization, mice were bled and antiserum was obtained. The specificity of each serum was confirmed by Western blot assays using recombinant polypeptides separated on 10% SDS-PAGE (30 µg/lane) and electrotransferred to nitrocellulose membranes. The membranes were then incubated with each immune serum (1:1000) in 2% non-fat dried milk, 0.05% Tween-20 in PBS pH 7.4 overnight at 4°C. Proteins were developed using peroxidase-conjugated secondary antibodies (1:5000, Zymed) and detected with the ECL-Plus system. Western blot assays using nuclear and cytoplasmic protein extracts from HM1-IMSS trophozoites were performed as described elsewhere [43].

Immunofluorescence confocal laser assays

Trophozoites were cultured on cover slides, fixed with 4% paraformaldehyde at 37°C for 40 min and permeabilized with 0.5% Triton-X100 in PBS 1× at 37°C for 40 min. Next, cells were blocked in 2% BSA for 60 min at 37°C, washed three times with PBS 1× and incubated with either anti-*EhCAF1* and anti-*EhAGO2-2* antibodies generated in the rabbit or anti-*EhXRN2*, and anti-*EhDCP2* antibodies generated in the mouse (1:200) at 37°C for 1 h. Cells were washed three times and incubated with fluorescein-labeled secondary antibodies (1:200) at 37°C for 1 h. Lastly, DNA was counterstained with 4′-6-diamidino-2-phenylindole (DAPI, 5 mg/ml) for 1 min. Samples were analyzed under an inverted microscope connected to a laser confocal scanning system (TCS SP2, Leica Microsystems).

Immunoprecipitation assays

The immunoprecipitation protocol was essentially that described in [44] with minimal modifications. Briefly, cytoplasmic proteins (50 µg) were diluted in 300 µl HNTG buffer (20 mM HEPES pH 7.5, 150 mM NaCl, 0.1% Triton, 10% glycerol) and incubated with 10 µl of protein G beads (Sigma) for 30 min at 4°C. Non-specifically interacting proteins were excluded by centrifugation at 3000 rpm at 4°C for 5 min. The supernatant was incubated with either anti-*EhCAF1* antibodies (1:100) or anti-*EhXRN2* antibodies (1:100) for 2 h at 4°C. Next, protein G-Sepharose beads were added to the samples and incubated for 16 h at 4°C. Immunoprecipitated proteins were collected by centrifugation, washed three times with HNTG buffer and then separated using 12% SDS-PAGE. Proteins were transferred to nitrocellulose membranes and detected by Western blot assays with rabbit anti-*EhCAF1* or mouse anti-*EhXRN2* antibodies.

Bacterial expression of double-stranded RNA and trophozoites transfection

Double-stranded RNA was obtained as described in [28]. Briefly, the *Ehpc4* full coding sequence (EHI_192520) was cloned into the *SmaI* and *XhoI* restriction sites of the pL4440 plasmid vector, which is flanked by T7 promoters [45]. Competent *E. coli* HT115 cells were transformed with pL4440-*Ehpc4* and spread onto LB-agar plates containing ampicillin and tetracycline. Isolated bacterial colonies were obtained after overnight culture at 37°C. Double-stranded RNA synthesis was induced by incubation with 2 mM IPTG for 4 h at 37°C. Cy3-labeling of purified dsRNA was performed with the Silencer siRNA labeling kit (Ambion), according to the manufacturer's instructions. The reaction mixture (containing 5 µg dsRNA, nuclease free-water, labeling buffer and Cy3 labeling reagent) was incubated for 1 h at 37°C in the dark. Labeled dsRNA was precipitated with ethanol, resuspended in DEPC-treated water and immediately used in colocalization assays.

RNA fluorescence *in situ* hybridization

To detect poly(A)⁺ RNA in fluorescence *in situ* hybridization (FISH) assays, parasites were harvested and allowed to adhere to microscope slides. Cells were fixed with 4% paraformaldehyde in PBS, denatured in 70% formamide at 70°C and incubated for 10 min with 25 mM NH₄Cl. The cells were permeabilized and

blocked for 30 min in 0.5% Triton X-100/2% BSA in PBS, followed by 2 h of prehybridization at room temperature in hybridization buffer (2% BSA, 4× SSC, 5% dextran sulfate, 35% deionized formamide and 10 U RNase inhibitor). Hybridization was performed overnight at room temperature in a humidified culture chamber in the presence of 300 ng/ml FITC-conjugated oligo-(dT)₃₀ in hybridization buffer. Slides were washed once in 4× SSC plus 35% deionized formamide and once in 4× SSC and were then counterstained with DAPI (1 mg/ml). Slides were mounted with Vectashield antifade (Vector). The subcellular localization was analyzed with a Leica TCS SP2 microscope. Merged images were obtained by superimposing image files using LCS Lite software (Leica Microsystems).

Supporting Information

Figure S1 XRN2 related proteins. (A) Multiple alignments of related XRN2 proteins. (B) Phylogenetic relationships between *EhXRN2* and XRN2 family members. The rooted tree was created with a neighbor-joining algorithm in the Mega 5.1 program, on the basis of ClustalW alignments of full amino acid sequences. Each protein's accession number is given in brackets. (PDF)

Figure S2 DCP2 related proteins. (A) Multiple alignments of related DCP2 proteins. (B) Phylogenetic relationships between *EhDCP2* and DCP2 family members. The rooted tree was created with a neighbor-joining algorithm in the Mega 5.1 program, on the basis of ClustalW alignments of full amino acid sequences. Each protein's accession number is given in brackets. (PDF)

Table S1 Predicted mRNA degradation proteins in *Entamoeba histolytica*. (PDF)

Table S2 Primers used in quantitative real-time PCR assays. (PDF)

Table S3 Comparison of *EhXRN2* with related proteins from several organisms. (PDF)

Table S4 Comparison of *EhDCP2* with related proteins from several organisms. (PDF)

Acknowledgments

We thank the Autonomous University of Mexico City for support and Dr. Upinder Singh (Stanford University, CA) for kindly providing the *Ehago2-2* gene clone.

Author Contributions

Conceived and designed the experiments: ILR EO LAM NG CPP CLC. Performed the experiments: ILR GGR CW ECT OHC. Analyzed the data: ILR LAM NG CPP CLC. Contributed reagents/materials/analysis tools: ILR EO GGR NG CW CPP CLC. Wrote the paper: ILR LAM CLC.

References

1. Bevilacqua A, Ceriani MC, Capaccioli S, Nicolini A (2003) Post-transcriptional regulation of gene expression by degradation of messenger RNAs. *J Cell Physiol* 195:356–372.
2. Chen CY, Shyu AB (2011) Mechanisms of deadenylation-dependent decay. *Wiley Interdiscip Rev RNA* 2:167–183.
3. Collier J, Parker R (2004) Eukaryotic mRNA decapping. *Annual Review of Biochemistry* Vol. 73: 861–890.
4. Lykke-Andersen S, Tomecki R, Jensen TH, Dziembowski A (2011) The eukaryotic RNA exosome: same scaffold but variable catalytic subunits. *RNA Biol* 8:61–66.

5. Kulkarni M, Ozgur S, Stoecklin G (2010) On track with P-bodies. *Biochem Soc Trans* 38:242–251.
6. Aizer A, Shav-Tal Y (2008) Intracellular trafficking and dynamics of P bodies. *Prion* 2:131–134.
7. Eulalio A, Behm-Ansmant I, Izaurralde E (2007) P-bodies: at the crossroads of post-transcriptional pathways. *Nat Rev Mol Cell Biol* 8:9–22.
8. Sen GL, Blau HM (2005) Argonaute 2/RISC resides in sites of mammalian mRNA decay known as cytoplasmic bodies. *Nat Cell Biol* 7:633–636.
9. Liu J, Rivas FV, Wohlschlegel J, Yates JR, Parker R, et al. (2005) A role for the P-body component GW182 in microRNA function. *Nat Cell Biol* 7:1261–1266.
10. Eulalio A, Behm-Ansmant I, Schweizer D, Izaurralde E (2007) P-Body Formation Is a Consequence, Not the Cause, of RNA-Mediated Gene Silencing. *Mol Cell Biol* 27: 3970–3981.
11. Sheth U, Parker R (2006) Targeting of aberrant mRNAs to cytoplasmic processing bodies. *Cell* 125: 1095–1109.
12. Cougot N, Babajko S, Séraphin B (2004) Cytoplasmic foci are sites of mRNA decay in human cells. *J Cell Biol* 165: 31–40.
13. Stalder L, Mühlemann O (2009) Processing bodies are not required for mammalian nonsense-mediated mRNA decay. *RNA* 7:1265–1273.
14. Chu CY, Rana TM (2006) Translation repression in human cells by microRNA-induced gene silencing requires RCK/p54. *PLoS Biol* 4(7):e210.
15. Stanley SL (2003) Amoebiasis. *Lancet* 361:1025–1034.
16. Abed M, Ankrí S (2005) Molecular characterization of *Entamoeba histolytica* RNase III and AGO2, two RNA interference hallmark proteins. *Exp Parasitol* 110:265–269.
17. Zhang H, Ehrenkaufer GM, Pompey JM, Hackney JA, Singh U (2008) Small RNAs with 5'-polyphosphate termini associate with a piwi-related protein and regulate gene expression in the single-celled eukaryote *Entamoeba histolytica*. *PLoS Pathog* 4:e1000219.
18. Zhang H, Pompey JM, Singh U (2011) RNA interference in *Entamoeba histolytica*: implications for parasite biology and gene silencing. *Future Microbiol* 6:1103–1117.
19. Weber C, Guigon G, Bouchier C, Frangeul L, Moreira S, et al. (2006) Stress by heat shock induces massive down regulation of genes and allows differential allelic expression of the Gal/GalNAc lectin in *Entamoeba histolytica*. *Eukaryot Cell* 5:871–875.
20. López-Camarillo C, Orozco E, Marchat LA, López-Camarillo C (2008) Transcriptional profile of the homologous recombination machinery and characterization of the EhRAD51 recombinase in response to DNA damage in *Entamoeba histolytica*. *BMC Mol Biol* 9:35.
21. Ramos E, Olivos-García A, Nequiz M, Saavedra E, Tello E, et al. (2007) *Entamoeba histolytica*: apoptosis induced in vitro by nitric oxide species. *Exp Parasitol* 116:257–265.
22. Parker R, Sheth U (2007) P bodies and the control of mRNA translation and degradation. *Mol Cell* 25:635–646.
23. Xiang S, Cooper-Morgan A, Jiao X, Kiledjian M, Manley JL, et al. (2009) Structure and function of the 5'→3' exoribonuclease Rat1 and its activating partner Rai1. *Nature* 458:784–788.
24. She M, Decker CJ, Svergun DI, Round A, Chen N, et al. (2008) Structural basis of dcp2 recognition and activation by dcp1. *Mol Cell* 29:337–49.
25. López-Camarillo C, de la Luz García-Hernández M, Marchat LA, Luna-Arias JP, Hernández de la Cruz O, et al. (2008) *Entamoeba histolytica* EhDEAD1 is a conserved DEAD-box RNA helicase with ATPase and ATP-dependent RNA unwinding activities. *Gene* 414:19–31.
26. Aizer A, Brody Y, Ler LW, Sonenberg N, Singer RH, et al. (2008) The dynamics of mammalian P body transport, assembly, and disassembly in vivo. *Mol Biol Cell* 19:4154–4166.
27. López-Camarillo C, Luna-Arias JP, Marchat LA, Orozco E (2003) EhPgp5 mRNA stability is a regulatory event in the *Entamoeba histolytica* multidrug resistance phenotype. *J Biol Chem* 278:11273–11280.
28. Solís CF, Santi-Rocca J, Perdomo D, Weber C, Guillén N (2009) Use of bacterially expressed dsRNA to downregulate *Entamoeba histolytica* gene expression. *PLoS One* 4:e8424.
29. Jagannath A, Wood MJ (2009) Localization of double-stranded small interfering RNA to cytoplasmic processing bodies is Ago2 dependent and results in up-regulation of GW182 and Argonaute-2. *Mol Biol Cell* 20:521–9.
30. Cassola A, De Gaudenzi JG, Frasch AC (2007) Recruitment of mRNAs to cytoplasmic ribonucleoprotein granules in trypanosomes. *Mol Microbiol* 65:655–670.
31. Schwede A, Ellis L, Luther J, Carrington M, Stoecklin G, et al. (2008) A role for Caf1 in mRNA deadenylation and decay in trypanosomes and human cells. *Nucleic Acids Res* 36:3374–3388.
32. Holecz FB, Correa A, Avila AR, Nakamura CV, Krieger MA, et al. (2007) Evidence of P-body-like structures in *Trypanosoma cruzi*. *Biochem Biophys Res Commun* 356:1062–1067.
33. Kederasha N, Anderson P (2002) Stress granules: sites of mRNA triage that regulate mRNA stability and translatability. *Biochem Soc Trans* 30:963–969.
34. Wilczynska A, Aigueperse C, Kress M, Dautry F, Weil D (2005) The translational regulator CPEB1 provides a link between dcp1 bodies and stress granules. *J Cell Sci* 118:981–992.
35. Kederasha N, Stoecklin G, Ayodele M, Yacono P, Lykke-Andersen J, et al. (2005) Stress granules and processing bodies are dynamically linked sites of mRNP remodeling. *J Cell Biol* 169:871–884.
36. Gilks N, Kederasha N, Ayodele M, Shen L, Stoecklin G, et al. (2004) Stress granule assembly is mediated by prion-like aggregation of TIA-1. *Mol Biol Cell* 15:5383–5398.
37. Brengues M, Teixeira D, Parker R (2005) Movement of eukaryotic mRNAs between polysomes and cytoplasmic processing bodies. *Science* 310:486–489.
38. Teixeira D, Sheth U, Valencia-Sanchez MA, Brengues M, Parker R (2005) Processing bodies require RNA for assembly and contain nontranslating mRNAs. *RNA* 11: 371–382.
39. Zhang H, Alramini H, Tran V, Singh U (2011) Nucleus-localized antisense small RNAs with 5'-polyphosphate termini regulate long term transcriptional gene silencing in *Entamoeba histolytica* G3 strain. *J Biol Chem* 286:44467–44479.
40. Takiff HE, Chen SM, Court DL (1989) Genetic analysis of the rnc operon of *Escherichia coli*. *J Bacteriol* 171:2581–2590.
41. Diamond LS, Harlow DR, Cunnick CC (1978) A new medium for the axenic cultivation of *Entamoeba histolytica* and other *Entamoeba*. *Trans R Soc Trop Med Hyg* 72:431–432.
42. Livak KJ, Schmittgen TD (2001) Analysis of relative gene expression data using real-time quantitative PCR and the 2^{-ΔΔC_T} Method. *Methods* 25:402–408.
43. Marchat LA, Gómez C, Pérez DG, Paz F, Mendoza L, et al. (2002) Two CCAAT/enhancer binding protein sites are cis-activator elements of the *Entamoeba histolytica* EhPgp1 (mdr-like) gene expression. *Cell Microbiol* 4:725–737.
44. Tovy A, Siman Tov R, Gaentzsch R, Helm M, Ankrí S (2010) A New Nuclear Function of the *Entamoeba histolytica* Glycolytic Enzyme Enolase: The Metabolic Regulation of Cytosine-5 Methyltransferase 2 (Dnmt2) Activity. *PLoS Pathog* 6:e1000775.
45. Timmons L, Court DL, Fire A (2001) Ingestion of bacterially expressed dsRNAs can produce specific and potent genetic interference in *Caenorhabditis elegans*. *Gene* 263:103–112.